High electronic excitation-induced crystallization in $Fe_{73.5}Cu_1Nb_3Si_{13.5}B_9$ amorphous alloy: II. Carbon cluster irradiation

2004 J. Phys.: Condens. Matter 16 1563

(http://iopscience.iop.org/0953-8984/16/9/005)

INSTITUTE OF PHYSICS PUBLISHING JOURNAL OF PHYSICS: CONDENSED MATTER

J. Phys.: Condens. Matter **16** (2004) 1563–1575 PII: S0953-8984(04)71425-3

High electronic excitation-induced crystallization in $Fe_{73.5}Cu_1Nb_3Si_{13.5}B_9$ amorphous alloy: II. Carbon cluster irradiation

G Rizza[1,4], A Dunlop[1], G Jaskierowicz[1], M Kopcewicz[2] and S Della-Negra[3]

[1] Laboratoire des Solides Irradiés, Commissariat à l'Energie Atomique/DRECAM/Ecole Polytechnique/CNRS, 91128 Palaiseau Cedex, France
[2] Institute of Electronic Materials Technology, Wolczynska 133, 01-919 Warszawa, Poland
[3] Institut de Physique Nucléaire (IPN), Orsay Campus, 91405 Orsay, France

E-mail: rizza@hp1sesi.polytechnique.fr

Received 6 November 2003
Published 20 February 2004
Online at stacks.iop.org/JPhysCM/16/1563 (DOI: 10.1088/0953-8984/16/9/005)

Abstract

We present a detailed study of the crystallization induced in an amorphous alloy by cluster ions. The formation of nanocrystalline iron boride phases was observed by transmission electron microscopy in an amorphous $Fe_{73.5}Cu_1Nb_3Si_{13.5}B_9$ alloy irradiated up to fluences of 1×10^9–2×10^{11} clusters cm^{-2} at room temperature with C_n ($n = 5$, 10, 60) carbon clusters at 20 MeV, but not after irradiation with C_{60} fullerenes at 30 MeV. The high level of energy deposited in electronic excitations along the path of carbon clusters induces radial pressure waves in the vicinity of the projectile trajectories. The formation of nanocrystallites was interpreted as being due to a structural relaxation which occurs in the wake of the shock front. The mechanical stresses induced by the pressure wave destabilize the amorphous structure and drive the nucleation of nanocrystallites.

1. Introduction

The recent discovery that high electronic energy deposition induces partial crystallization in an amorphous alloy [1] put back in discussion the general conviction that the effect of swift heavy ion irradiation on metallic glasses was limited only to the anisotropic growth of the target [2–7]. This latter effect concerns all the amorphous targets submitted to high electronic energy deposition, and was observed above a threshold energy deposition, $S_e \sim 10\,keV\,nm^{-1}$, and above a critical irradiation fluence, Φ_c. During the anisotropic growth the sample shrinks along the beam direction and expands perpendicularly to the beam direction.

[4] Author to whom any correspondence should be addressed.

The discovery of the irradiation-induced crystallization of a metallic glass has opened a novel investigation on swift heavy ion modification of matter. In a companion paper, this phenomenon was studied in detail after irradiation of amorphous $Fe_{73.5}Cu_1Nb_3Si_{13.5}B_9$ alloy with monoatomic projectiles. In order to complete our study, in this paper we analyse the behaviour of the same amorphous alloy under cluster ion irradiation.

Using a mono-atomic projectile the maximum linear rate of energy deposited in electronic excitation and ionization is usually limited to about 40 keV nm^{-1} for a swift heavy ion in the gigaelectronvolt region. Irradiation with cluster ions (such as fullerenes in the 20–40 MeV range) permits us to overcome this limitation and to reach linear rates of energy deposition in electronic processes up to 80 keV nm^{-1}. Moreover, the density of energy deposited into the target is much higher for cluster ions. This is because the volume in which the energy is deposited scales with the range of the δ-electrons, which depends only on the projectile velocity. The higher the ion velocity, the lower the density of energy deposited on the electronic system. For equivalent linear rates of energy loss by megaelectronvolt clusters and by gigaelectronvolt heavy ions, the velocity of the cluster ions is one order of magnitude lower than that of mono-atomic ions, so that the energy density around the projectile path can be at least one order of magnitude higher in the case of cluster ions than that obtained for mono-atomic projectiles [8]. As a consequence, the relaxation of such a high energy density may induce strong structural changes in the targets [9].

The Fe-based amorphous alloys formed by rapid solidification of a metallic melt are of a considerable technological interest for their high saturation magnetization and low coercitivy. The magnetic properties of the amorphous alloys are very sensitive to their microstructure. It has been reported that the bcc structure with nanoscale grain size can be formed in amorphous FeSiB-based alloys containing Cu and Nb by utilizing the first stage of the crystallization process [10–13]. The first experiments performed by Yoshizawa *et al* [10] for the $Fe_{73.5}Cu_1Nb_3Si_{13.5}B_9$ alloy have shown that annealing the amorphous alloy at a temperature between 520 and 650 °C leads to the formation of the nanocrystalline bcc-Fe(Si) phase with well defined homogeneous grains, with a typical size of 10–15 nm, embedded in the retained amorphous structure. The formation of the bcc-Fe(Si) nanostructure in the FeCuNbSiB system was explained by the combination of an increasing nucleation rate of the bcc phase resulting from the immiscibility of Cu to Fe and a reduced crystal growth rate to the small diffusivity of Nb in Fe. The increase of the annealing temperature above the second crystallization peak (at about 670 °C) in the differential scanning calorimetry (DSC) curve causes a complete crystallization of the amorphous matrix as a result of which iron borate compounds (Fe_2B, Fe_3B, $Fe_{23}B_6$, ...) are formed, the size of crystalline Fe(Si) grains increases and the soft magnetic properties dramatically deteriorate.

As this alloy is characteristic of a particular class of amorphous alloys exhibiting two-step crystallization, it seems interesting to study the behaviour of such an alloy submitted to high electronic energy deposition. Thus, the aim of this paper is to draw a general scheme for the irradiation-induced crystallization in the $Fe_{73.5}Cu_1Nb_3Si_{13.5}B_9$ amorphous alloy under high electronic energy deposition.

2. Experimental details

The samples used in this study are amorphous $Fe_{73.5}Cu_1Nb_3Si_{13.5}B_9$ ribbons prepared by the melt spinning technique. The targets in the form of 3 mm diameter discs have been electrochemically prethinned for transmission electron microscopy (TEM) observations. The amorphous nature of the as-spun ribbons was verified using Mössbauer and TEM techniques.

Cluster irradiation was performed using the Tandem accelerator facility of Nuclear Physics Institute in Orsay (France). The specimens were irradiated at normal incidence and at 300 K

Table 1. Characteristics of the irradiation conditions with megaelectronvolt cluster ions: projectile, ion energy (E), fluence (Φ), projected range (R_p), average linear rate of energy deposition in nuclear (S_n) and electronic (S_e) processes, relative velocity of the clusters ($\beta = v/c$), and diameter of damaged regions (D). In the last column the most probable crystalline phase is reported.

Projectile	E (MeV)	Φ (ions cm^{-2})	R_p (μm)	S_n (keV nm^{-1})	S_e (keV nm^{-1})	β (%)	D (nm)	Possible phase
C_5	20	1×10^{11}	2.15	3.3×10^{-2}	12.3	2.7	4	Amorphous
C_{10}	20	1×10^{10}	1.34	0.15	23	1.9	10	$Fe_{23}B_6$ Fe_2B
C_{60}	20	1×10^{10}	0.37	2.5	60	0.7	14	$Fe_{23}B_6$ Fe_2B
C_{60}	30	1×10^{10}	0.51	1.9	79	0.9	13	Amorphous

with C_5, C_{10} and C_{60} cluster ions at 20 MeV and with C_{60} cluster ions at 30 MeV. The flux was about 10^5 clusters cm^{-2} s^{-1} on a 7 mm^2 surface. The irradiation fluence is 1×10^{11} ions cm^{-2} for the irradiation with C_5 carbon clusters and 10^{10} ions cm^{-2} for C_{10} and C_{60} cluster ions at 20 MeV and for C_{60} cluster ions at 30 MeV.

Observations of amorphous targets irradiated with swift heavy ions allowed the visualization by TEM analysis of the surface deformations on both sample surfaces [14, 15]. These permitted the determination of the cross-sections of the cylinders of *modified* matter. The irradiation-induced microstructural evolution of our samples was studied using a 300 keV Philips CM30 transmission electron microscope. TEM observations were performed using the phase contrast technique, which consists of defocusing the objective lens of the microscope to give rise to a phase contrast (Fresnel fringes) inside the ion deformed regions (tracks). High resolution transmission electron microscopy (HRTEM) micrographs were processed with a slow scan CCD camera and analysed with the Digital Micrograph program. The TEM observations were always performed using a very low electron flux in order to avoid any structural modification of the sample induced by the electron beam.

3. Experimental results using MeV cluster ions

The characteristics of the irradiation conditions are reported in table 1: the projectiles used, the incident energy (E) and fluences (Φ), the projected range of the clusters ions (R_p), the linear rates of energy deposition in nuclear (S_n) and in electronic (S_e) processes, the relative velocity of the clusters (β), and the mean track diameter (D).

The value of the deposited energy has been calculated using the SRIM2000 Code [16]. Theoretical and experimental results indicate that the energy loss per carbon atom in a cluster is approximately that of an individual carbon ion of the same velocity [17]. In other words, the linear rate of deposited energy can be obtained by simply multiplying the value of the linear rate of deposited energy per atom by the number of atoms composing the molecule, i.e. it will scale with the Z-cluster number. The relative velocity β of the projectile is expressed as a percentage of the velocity of light.

In the first part of this paper, we will analyse the evolution of the latent track diameter as a function of the nature of the cluster ions. In the second part, we will focus our study on the phenomenon of the crystallization induced by high electronic energy deposition.

3.1. Latent track formation

Figure 1(a) shows an HRTEM micrograph of an unirradiated sample. As expected, only the amorphous structure is observed. This is confirmed by the corresponding electron diffraction

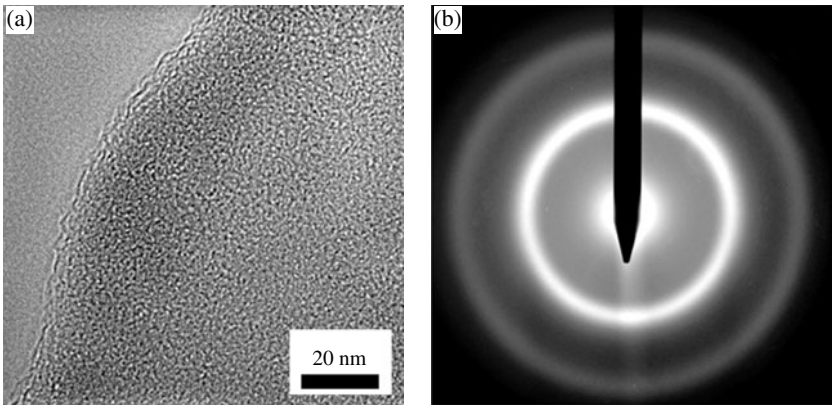

Figure 1. Bright field micrograph of the amorphous structure of the unirradiated sample (a). The corresponding diffraction pattern plot is shown in (b).

pattern (figure 1(b)). It consists of two very wide diffraction rings. The average distance x_m in the amorphous structure is calculated using the Guinier formula [20] and considering the first amorphous ring, $x_m = 1.23d = 2.50$ Å. This value agrees with the determination of Hampel *et al* [21], giving $x_m = 2.5$ Å.

Figures 2(a)–(d) show conventional TEM images of latent tracks induced by C_n ($n = 5$, 10, 60) fullerenes at 20 MeV and by C_{60} carbon clusters at 30 MeV. All images allow the density of the tracks as well as the track diameter to be determined. The tracks are randomly distributed all over the surface of the sample and their density is consistent with the irradiation fluence, i.e. each projectile induces visible damage in the metallic glass. The diameter of the cluster impacts was measured in conventional TEM mode considering the inner diameter of the track. This is because the inner diameter is invariant with respect to the defocalization of the microscope lens. For the sample irradiated with C_5 fullerenes an accurate measurement of the diameter of the tracks is difficult. This is because of their very discontinuous appearance and their low phase contrast.

The diameter of the impact regions, averaged over a large number of tracks, scales from 4 nm for the irradiation with C_5 clusters, up to 10 and 14 nm, for the irradiation with 20 MeV C_{10} and C_{60} clusters, respectively. The measured diameter for the C_{60} fullerenes at 30 MeV is about 13 nm.

The evolution of the latent track diameter as a function of the linear rate of electronic energy deposition, S_e, is shown in figure 3. For comparison, the experimental results obtained for the monoatomic projectiles (Pb ions at 700 MeV and 5 GeV) are also shown. The diameter of the latent tracks induced at 300 K by cluster ions regularly increases with the linear rate of energy deposition in electronic processes, S_e. The dashed curve does not represent a curve fit line, but is just to help the eye to follow the diameter evolution.

In our experimental set-up the velocities of all the cluster ions and of 700 MeV Pb ions lie on the low velocity side of the stopping power curve. On the other hand, the velocity corresponding to the irradiation with 5 GeV Pb ions lies on the high velocity side of the stopping power curve. Previous results demonstrated that there is not a simple relation between the linear rate of electronic energy deposition, S_e, and the latent track diameter. For a given projectile, the track diameter increases with the ion velocity, reaches a maximum value, and then decreases again beyond the stopping power maximum, giving rise to a hook-like curve [18]. This effect is often called the velocity effect [19], indicating that for the same S_e, slow projectiles induce

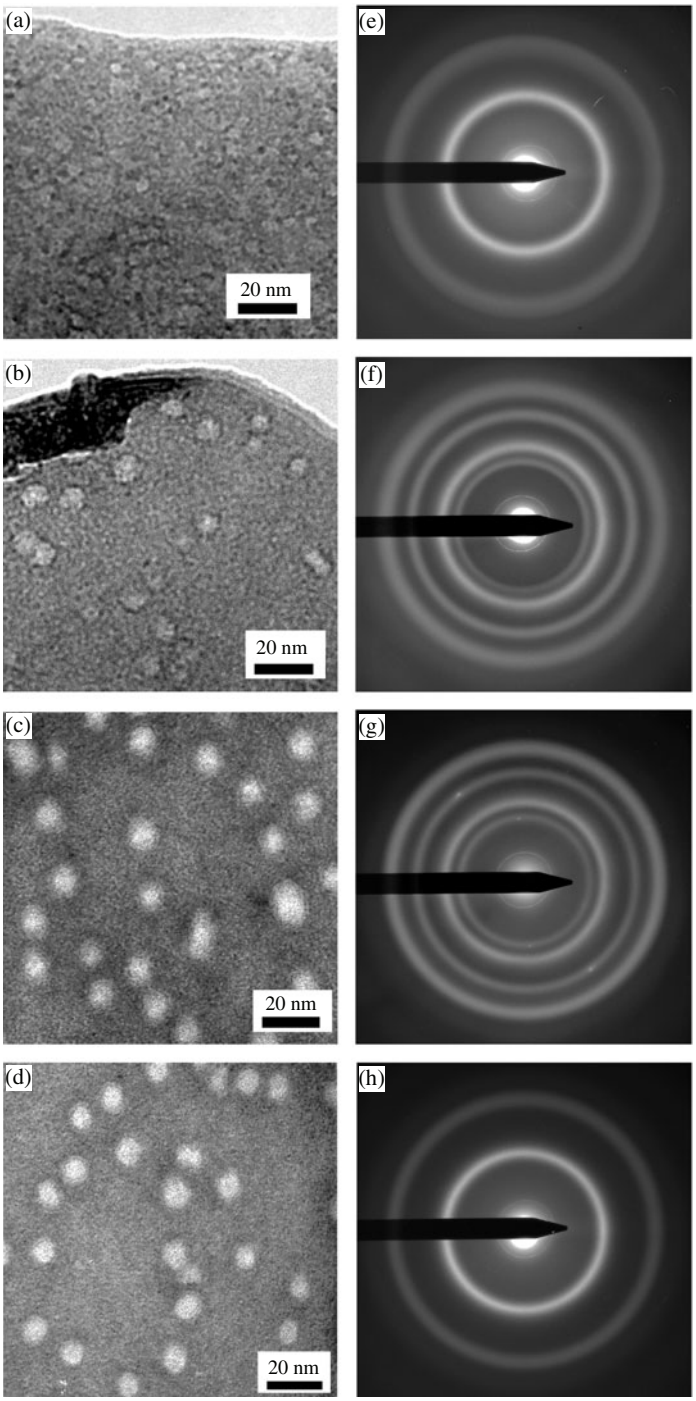

Figure 2. Bright field transmission electron micrographs in slightly defocused conditions in a $Fe_{73.5}Cu_1Nb_3Si_{13.5}B_9$ amorphous sample irradiated at 300 K with 20 MeV C_5 cluster ions (a), C_{10} (b) and C_{60} (c) cluster ions and with 30 MeV C_{60} cluster ions (d). The corresponding diffraction patterns are shown in (e)–(h). The irradiation fluence is 1×10^{11} ions cm^{-2} for the irradiation with C_5 carbon clusters and 10^{10} ions cm^{-2} for C_{10} and C_{60} cluster ions at 20 MeV and for C_{60} cluster ions at 30 MeV.

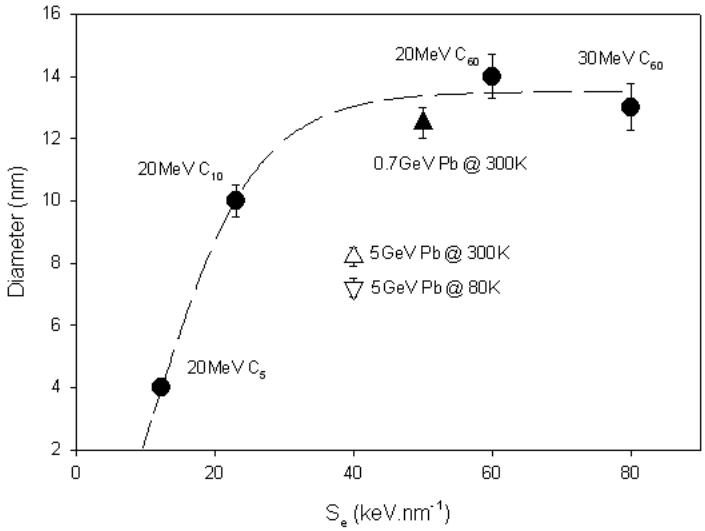

Figure 3. The plot shows the evolution of the inner track diameter as a function of the deposited energy S_e. Circles and triangles represent cluster and monoatomic ions, respectively. Filled and open symbols represent low and high velocity projectiles, respectively.

larger diameter tracks than faster projectiles due to the differences in the density of deposited energy by low and high velocity ions. The higher the δ-electron velocity, the larger their range, and the lower the energy density deposited on the electron systems as the ion damaged volume scales with the range of the δ-electrons. The major importance of the velocity of the projectile in the resulting damage is confirmed by the fact that all the points related to the carbon cluster irradiation lie on the same curve (dashed curve in figure 3) as well as the point corresponding to low velocity Pb ions. On the other hand, as expected, the points corresponding to high velocity Pb ions at 5 GeV are located below this curve.

The threshold value of energy transfer for visible track creation (S_e^t) can be estimated using the point of intersection of the dashed curve with the energy axis. This corresponds to the threshold value for the creation of tracks visible by TEM [15]. The threshold value is about $S_e^t \sim 10$ keV nm^{-1}. Rather than the linear rate of energy deposition, the energy density is the relevant parameter governing the track formation [9]. The energy density required for the creation of visible tracks can be estimated using the following simple relation [14]:

$$\Pi = [4/(\pi D^2)]S_e \text{ (eV nm}^{-3}) \tag{1}$$

where S_e represents the linear rate of energy deposition into electronic processes and D the track diameter. Using the track diameter measured for C_5 cluster irradiation ($D \sim 4$ nm) and the energy threshold for track formation ($S_e^t \sim 10$ keV nm^{-1}), the threshold of the energy density for track formation can be estimated to be $\Pi \approx 800$ eV nm^{-3}.

3.2. Irradiation-induced crystallization

In this second part of the paper we will analyse the phenomenon of the crystallization induced by high electronic energy deposition.

3.2.1. Irradiation at 300 K with C_n ($n = 5, 10, 60$) carbon clusters at 20 MeV. The electron diffraction patterns (DPs) corresponding to the $Fe_{73.5}Cu_1Nb_3Si_{13.5}B_9$ amorphous alloy

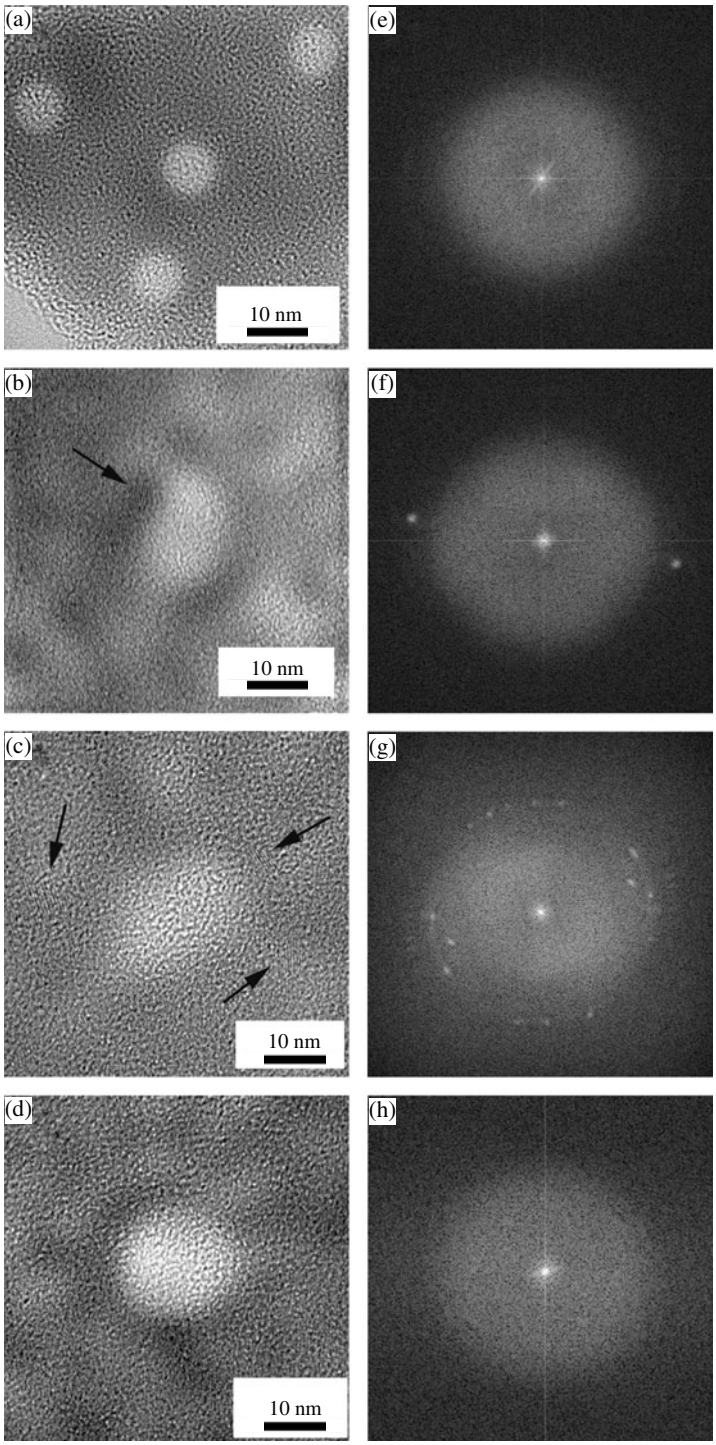

Figure 4. High resolution transmission electron microscopy (HRTEM) of the metallic glass irradiated at 300 K with 20 MeV C_5, C_{10} and C_{60} and with 30 MeV C_{60} carbon clusters, respectively ((a)–(d)). Nanocrystallites are indicated by arrows. Corresponding Fourier transform plots are presented in ((e)–(h)).

irradiated respectively with C_5, C_{10} and C_{60} at 20 MeV, are shown in figures 2(e)–(g). HRTEM micrographs are shown in figure 4.

The DP corresponding to the alloy irradiated with 20 MeV C_5 carbon clusters (figure 2(e)) is characteristic of an amorphous structure, where only two diffuse diffraction rings are visible. No additional rings, characteristic of a crystalline structure, were observed. This feature has been verified on a large number of micrographs and it is confirmed by the HRTEM analysis (figure 4(a)). The HRTEM micrograph shows that both the track core and the surrounding matrix appear as amorphous. Different contrast between track core and surrounding matrix is ascribed to the amorphous structure modification in the vicinity of the ion path due to the electronic relaxation. The amorphous structure of the sample is confirmed by the corresponding Fourier transform (FT) plot as shown in figure 4(e). The fact that the irradiation with 20 MeV C_5 carbon clusters does not induce phase transformation in the alloy suggests the existence of a threshold value for the electronic energy deposition required to induce the crystallization.

Figures 2(f), (g) show the DPs corresponding to 20 MeV C_{10} and C_{60} carbon cluster irradiation, respectively. In both cases, besides the two diffuse amorphous rings, new narrow rings appear. These rings are the signature of a partial crystallization of the amorphous alloy due to the high electronic energy deposition. In figure 2(f) (C_{10} clusters) a narrow crystalline ring is found inside the first amorphous ring, whereas a second more diffuse ring is found between the first and the second amorphous ring. The presence of two crystalline rings is also observed in figure 2(g) (20 MeV C_{60}). The first new ring is found inside the first amorphous ring and the second between the first and the second amorphous rings. With respect to the irradiation with C_{10} clusters, the new rings present a better defined crystalline structure with the appearance of intense diffraction spots.

The HRTEM micrographs show the presence of nanocrystalline structures in targets irradiated with 20 MeV C_{10} and C_{60} aggregates (figures 4(b), (c)). The nanoscale grains are inhomogeneously distributed both in the close vicinity of the track core and a few nanometres away from it ($\sim$5 nm). The size of the nanocrystallites ranges between 1 and 4 nm.

The most probable crystalline phases from which the diffraction rings originate, measured on several diffraction patterns, have been reported in table 1. The observed nanophases are compatible with both $Fe_{23}B_6$ and Fe_3B structures and no evidence of the nucleation of the Fe(Si) phase was found. We observe mainly the nanocrystallization of phases which are characteristic of the second crystallization step.

3.3. Irradiation at 300 K with C_{60} fullerenes at 30 MeV

More puzzling is the result of the DP plot corresponding to the 30 MeV C_{60} carbon cluster irradiation (figure 2(h)). In the DP plot only the two diffuse amorphous rings are visible and no additional rings, corresponding to a crystalline phase, were detected. In the HRTEM micrograph (figure 4(d)), the lighter contrasts correspond to the latent track core and the darker contrast to the surrounding matrix. No sign of the formation of nanocrystallites has ever been observed in the studied samples. The amorphous structure of the alloy is confirmed by the corresponding FT plot, where only a diffuse ring is visible (figure 4(h)).

This result is quite surprising. As the linear rate of energy deposition in electronic processes during 30 MeV C_{60} ion irradiation is 30% larger than that deposited using 20 MeV C_{60} ions, we could expect to observe a stronger crystallization effect. The experimental evidence that crystallization does not occur for very high energy deposition seems to indicate that an upper energy deposition threshold exists concerning crystallization.

4. Discussion

If the thermal treatment is the most frequently used method to induce the crystallization of an amorphous alloy (see e.g. [10–13]), crystallization can also be obtained under mechanical stress. Nanocrystallization under mechanical stress was observed in mechanical milling [22], nanoindentation [23] and shock loading [24] experiments. Crystallization can also be induced by external factors such as electron and neutron irradiation [25, 26].

In this paper we deal with a new method: the crystallization induced by swift heavy ion irradiation.

In order to understand the mechanism of the irradiation induced nanocrystallization in the $Fe_{73.5}Cu_1Nb_3Si_{13.5}B_9$ amorphous alloy, it is useful to review some aspects of the relaxation of the energy deposited into the target during the slowing-down of a swift heavy ion through matter.

The passage of a swift ion through matter mainly leads to the electronic excitation and ionization of target atoms ($\leqslant 10^{-17}$ s). During this process showers of excited δ-electrons are ejected around the projectile path and a very high space-charge density is created ($\sim 10^{-15}$ s). In metallic systems, the lifetime of space charge is limited due to the rapid screening by the conduction electrons ($\sim 10^{-13}$ s). The residual damage depends on the nature of the target and on the amount of energy deposited into electronic processes (S_e).

In order to understand how the deposited energy into an electronic system can be transferred to the atomic subsystem, different models were proposed. Following the timescale of events, the Coulomb explosion models deal with the excitation and ionization of the electrons in the vicinity of the ion path and the conversion of the resulting electrostatic potential energy into kinetic energy [27–30]. The thermal spike models deal with the conversion of the energy of the ejected δ-electrons into atomic displacements [31–34].

In the Coulomb explosion model, atoms located in the close vicinity of the ion path receive a radial impulse. The original ion-explosion-spike model was proposed by Fleischer *et al* [27] to account for damage creation in insulators. In insulators, the electrostatic potential energy resulting from the ionization of the atoms is not screened. The recoil energy E_r due to the Coulomb repulsion can reach a high value (up to a few 10 eV), which is sufficient to induce individual atomic displacements. In metallic targets, the efficient screening of positive charges by the free conduction electrons makes such individual processes inefficient. However, a Coulomb explosion model has been applied to metallic targets when the space charge resulting from the ionization of the atoms is continuous along the ion path [30]. The cylinder of highly ionized matter surrounding the ion path is very unstable. The radial kinetic energy E_r conveyed to the charged ions through Coulomb repulsion depends mainly on the density and lifetime of the space charge. In metallic systems, the lifetime of the space charge is limited by the response of the conduction electrons to an electrostatic perturbation. Time t related to plasma frequency ω_p ($t \geqslant \omega_p^{-1} \sim 10^{-16}$ s) is much shorter than the characteristic phonon vibration time (10^{-13} s). The radial impulse received by all atoms in the vicinity of the ion path corresponds to $E_r \sim 0.1$ eV to a few electronvolts, a much smaller amount than in insulators. But due to the very short time (a few 10^{-17} s) spent by an ion to travel an interatomic distance, all the atoms lying in the vicinity of the ion trajectory are collectively repelled in a coherent way. The radial shock wave that is generated might favour damage creation in metals.

The thermal spike model was originally proposed by Seitz and Koehler [31], then developed by Toulemonde and co-workers [35–37]. In this model, the electronic excitation and ionization along the ion track results in thermalization of excited electrons. The energy is then transferred by *electron–phonon* coupling to the atomic subsystem within 10^{-13}–10^{-10} s. For intense electronic excitations and efficient electron–phonon coupling a cylindrical region

around the ion track will melt. The heat transfer from the electronic to the atomic subsystem is deduced from the numerical solution of a set of coupled differential equations [35, 37].

An alternative thermal spike model was proposed by Volkov and Borodin [38, 39] for monoatomic projectiles in the gigaelectronvolt region. In this model, the heating transfer from the thermalized electrons into the atomic subsystem occurs via *electron–ion* energy exchange. Numerical estimations of the lattice heating up in the monoatomic ion track indicate that the temperature increase is insufficient to melt the majority of metallic materials.

For Johnson *et al* [29] the rapid rise of the potential energy due to the ion-deposited energy, converted into centre of mass motion, results in a radial pressure gradient. The individual impulses are described by a local energy density (ε) and its gradient ($-\nabla(\varepsilon)$).

Very recently, Bringa and Johnson [40], using molecular dynamic simulations of electronic sputtering, showed that a heat spike can be thought of as the final result of a Coulomb explosion energy conversion mechanism. They show that at high excitation density the primary effect of a repulsive energy (Coulomb explosion or pulse wave) is the production of a cylindrical heat spike. Therefore, for the authors, the Coulomb explosion and the thermal spike are the early and the late aspects of the same process.

4.1. Which process for the swift heavy ion-induced crystallization?

Because the timescale relative to the conversion of the energy of the projectile into atomic movement is not directly accessible by any technique, the origin of the irradiation-induced crystallization process, e.g. thermal or mechanical, may only be deduced from indirect experimental observations.

Is the irradiation-induced crystallization a pure thermal process? In the thermal spike model, energy deposition into the electronic system gives rise to an increase of the temperature in the close vicinity of the ion trajectory. If the temperature is the driving force for the crystallization, an increase of the temperature has to enhance the atomic mobility, and thus nucleation and growth of the nanocrystallites. As in thermal spike models, the higher the density of energy deposited in the electronic system, the higher the temperature increase, and the stronger the crystallization effect should be. Thus, we expect the higher effects after irradiation with 30 MeV C_{60} ions. Since the alloy remains amorphous after 30 MeV C_{60} ion irradiation, this gives us a first indication that the temperature is not the only parameter governing the crystallization process.

Another way to check if the irradiation-induced crystallization has a thermal origin is to estimate the value of the diffusion coefficient, D, and to compare it with the diffusion coefficient for metallic glasses. The diffusion coefficient for our irradiation conditions is simply estimated to be $D \sim L^2/4t$, where L is the distance from the ion trajectory at which nanocrystallites were found and t the characteristic time for cooling down of the heated region. The distance L is $L \sim$ 5–15 nm [1]. On the other hand, since the different thermal spike models predict different values for the temperature increase, the characteristic time t for electronic relaxation will depend on the model.

In the framework of the thermal spike models based on electron–phonon coupling [34, 36], it is assumed that for a high value of the stopping power a melted region is formed around the ion path. In this case, the diffusion coefficient has to be calculated in a liquid phase and t corresponds to the lifetime of the molten phase. According to Toulemonde *et al* [34], the lifetime of the molten ion track for the $Fe_{85}B_{15}$ alloy is of the order of 2×10^{-11} s for a stopping power of 60 keV nm^{-1}. As the $Fe_{85}B_{15}$ alloy composition is not too different from the alloy studied by us, we take this value as a good estimation of the lifetime of the melted phase

during our irradiations. If the nanocrystallites nucleated in a melted region, the corresponding diffusion coefficient should then be of the order of $D \sim 10^{-5}$–10^{-6} m^2 s^{-1}. This value is at least two orders of magnitude larger than the diffusion coefficient of a metallic glass measured above the melting point, 10^{-8}–10^{-10} m^2 s^{-1} [41].

In the thermal spike model based on electron–atom interaction, the temperature increase does not lead to a local melting of the sample. In this case, the diffusion coefficient has to be calculated in a solid phase, and the characteristic time t will correspond to the complete electronic relaxation, 10^{-9} s [42]. In this case, the calculated diffusion coefficient is $D \sim 10^{-8}$ m^2 s^{-1}. This value has to be compared to the diffusion coefficient in a solid phase as measured in isothermal annealing experiments [43]. The experimental values for the ^{59}Fe isothermal tracer diffusion coefficient at 633 and 673 K in unrelaxed $Fe_{91}Zr_9$ and $Fe_{78}Si_9B_3$ alloys are $D \sim 10^{-17}$ and $\sim 10^{-19}$ m^2 s^{-1}, respectively. Again in this approach the experimental values are orders of magnitude lower than our estimation.

Crystallization cannot be a diffusive process because the relaxation time of the electronic state is too fast to allow long-range atomic diffusion.

Another indication of the fact that thermal effects do not play a major role in the crystallization process can be deduced from the fact that if the irradiation-induced crystallization was a thermally activated process, we should find the crystalline phases corresponding to the primary crystallization: specifically the Fe(Si) phase. Nevertheless, not only was no evidence for the formation of the Fe(Si) phase found, but we mainly observe the precipitation of borate compounds, which are typical of the second crystallization step.

We finally want to indicate that irradiation-induced crystallization may just concern amorphous alloys that crystallize in two steps. In fact after irradiation of a 'conventional' amorphous alloy ($Fe_{40}Ni_{35}Si_{10}B_{15}$) with Pb ions using the GANIL accelerator, no sign of crystallization was detected by TEM after irradiation at fluences of 1×10^{11} and 1×10^{12} ions cm^{-2}. It was found that this alloy follows the usual behaviour, so that only surface deformations could be seen by TEM [44]. These two types of amorphous alloys have similar melting temperatures, thermal conductivities and crystallization temperatures ($\sim$520 °C) [12, 13, 45]. The only relevant difference is that amorphous $Fe_{40}Ni_{35}Si_{10}B_{15}$ alloy crystallizes in one step. The different crystallization behaviours of these two types of amorphous alloys could also be related to the presence of copper atoms which act as nucleation centres in the crystallization process.

From the previous results we conclude that, although a local heating of the sample exists, it cannot account for the formation of the observed nanocrystalline phases.

Is the irradiation-induced crystallization a mechanical process? The recent discovery that nanocrystallization in metallic glasses can be obtained during high energy ball milling, nanoindentation and shock compression experiments, has highlighted the importance of the stress and strain on the crystallization process as opposed to crystallization by thermal annealing. In this viewpoint, we will try to see if irradiation-induced nanocrystallization may be driven by a mechanical stress.

All the proposed mechanisms describing how the excitation and ionization energy deposited by an incident fast ion can be converted into atomic movement predict that, in the cylindrical track, the atoms are highly excited, having a large number of internal degrees of freedom. A fraction of this internal energy can be converted into centre of mass motion in a short time. This gives rise to a transiently pressurized cylindrical disturbance, referred to as a pressure pulse or a shock wave, which is followed by a time-dependent acoustic wave within about 10^{-15} s. When a shock wave is loaded, both mechanical effects and temperature effects are produced [40].

In the close vicinity of the ion path, the electronic relaxation can be seen as a centre of expansion, that can be figured out both as a visco-elastic inclusion [46, 47] or an excess of free volume zone [7]. Simultaneously, centres of compression are created in the material. These regions are local regions of increased density which travel through the material as an elastic shock wave. As the packing density of atoms in metallic glasses is slightly smaller (by $\sim$2%) than that of ordered arrangements, one might expect that the application of an external pressure could induce crystallization in metallic glasses since they can be compacted during shock loading [48].

Based on the idea that density fluctuations exist in amorphous alloys [49], irradiation-induced crystallization may thus be driven by a collective and coherent motion of atoms towards low density regions due to the propagation of the outgoing pressure wave.

When a shock wave is loaded, mechanical effects are produced in the wake of the shock wave. During this fast process, the phase which nucleates first is not necessarily the most stable thermodynamically (Fe(Si) in our case), but rather the most kinetically accessible one (Ostwald's rule of stages [50]).

As a consequence of the frustration of the system to reach the equilibrium phase, the phase that forms has the lowest free energy barrier for nucleation during shock loading ($Fe_{23}B_6$ in our case) [51]. Metastable phases can thus can be created by this process [52, 53].

Beyond the densification of the metallic glass, the pressure application also results in the reduction of the atomic mobility [54]. This second effect goes towards a reduction of the crystallization process. Thus, we interpret the experimental evidence that irradiation with 30 MeV C_{60} ions does not induce crystallization in $Fe_{73.5}Cu_1Nb_3Si_{13.5}B_9$ alloy as follows. According to the Coulomb explosion model, the pressure developed by the shock wave is a function of the energy deposited into the electronic system. The crystallization rate is thus given by the competition between densification-driven crystallization and pressure-induced decrease of the atomic mobility. When the deposited energy is higher than a threshold value, for which the atomic mobility is almost completely suppressed, the atomic rearrangement is inhibited and the phase transformation does not occur. In this case the alloy remains amorphous.

5. Conclusion

The effect of the swift heavy ions on the crystallization in $Fe_{73.5}Cu_1Nb_3Si_{13.5}B_9$ amorphous alloy investigated by means of TEM analysis were discussed. It has been shown that the high level of energy deposition into electronic system leads to the partial crystallization of the amorphous alloy, and that the crystalline phase is a metastable phase. We showed that the crystallization process cannot be explained as resulting only from a local *temperature increase*. We proposed a qualitative interpretation based on the effect of an irradiation-induced pressure wave.

Acknowledgments

The authors would like to thank all the staff of the IPN Orsay for their help during the irradiation.

References

[1] Dunlop A, Jaskierowicz G, Rizza G and Kopcewicz M 2003 *Phys. Rev. Lett.* **90** 015503
[2] Klaumünzer S, Schumacher G, Rentzsch S, Vogl G, Soldner L and Bieger H 1982 *Acta Metall.* **30** 1493
[3] Audouard A, Balanzat E, Fuchs G, Jousset J C, Lesueur D and Thomé L 1987 *Europhys. Lett.* **3** 327
Audouard A, Balanzat E, Fuchs G, Jousset J C, Lesueur D and Thomé L 1989 *Nucl. Instrum. Methods* B **39** 18

[4] Klaumünzer S, Li C, Loffler S, Rammensee M, Schumacher G and Neitzert H Ch 1989 *Radiat. Eff. Defects Solids* **108** 131
[5] Audouard A, Toulemonde M, Szenes G and Thomé L 1998 *Nucl. Instrum. Methods* B **146** 233
[6] Hou M D, Klaumünzer S and Schumacher G 1990 *Phys. Rev.* B **41** 1144
[7] Audouard A, Balanzat E, Jousset J C, Lesueur D and Thomé L 1993 *J. Phys.: Condens. Matter* **5** 995
[8] Bouffard S, Leroy C, Della-Negra S, Brunelle A and Costantini J M 2001 *Phil. Mag.* A **81** 2841
[9] Dammak H, Dunlop A, Lesueur D, Brunelle A, Della-Negra S and Beyec Y 1995 *Phys. Rev. Lett.* **74** 1135
[10] Yoshizawa Y, Oguma S and Yamauchi K 1988 *J. Appl. Phys.* **64** 6044
[11] Gorria P, Garitaonandia J S and Barandiaran J M 1996 *J. Phys.: Condens. Matter* **8** 5925
[12] Kataoka N, Inoue A, Masumoto T, Yoshizawa Y and Yamauchi K 1989 *Japan. J. Appl. Phys.* **28** 1820
[13] Kulik T and Hernando A 1995 *Mater. Sci. Forum* **179–181** 587
[14] Dunlop A, Jaskierowicz G and Della-Negra S 1997 *C. R. Acad. Sci.* II b **325** 397
[15] Dunlop A, Henry J and Jaskierowicz G 1998 *Nucl. Instrum. Methods* B **146** 222
[16] Ziegler J F, Biersak J P and Littmark U 1985 *Stopping Power and Ranges of Ions in Matter* vol 1 (New York: Pergamon)
[17] Baudin K, Brunelle A, Chabot M, Della-Negra S, Depauw J, Gardés D, Hakansson P, Le Beyec Y, Billebaud A, Fallavier M, Remillieux J, Poizat J C and Thomas J P 1994 *Nucl. Instrum. Methods* B **94** 341
[18] Jensen J, Dunlop A, Della-Negra S and Toulemonde M 1998 *Nucl. Instrum. Methods* B **146** 412
[19] Meftah A, Brisard F, Costantini J M, Hage-Ali M, Stoquert J P, Studer F and Toulemonde M 1993 *Phys. Rev.* B **48** 920
[20] Guinier A 1964 *Théorie et Technique de la Radiocristallographie* (Paris: Dunod) p 452
[21] Hampel G, Pundt A and Hesse J 1992 *J. Phys.: Condens. Matter* **4** 3195
[22] Trudeau M L, Schulz R, Dussault D and Van Neste A 1990 *Phys. Rev. Lett.* **64** 99
[23] Kim J J, Choi Y, Suresh S and Argon A S 2002 *Science* **295** 654
[24] Liu Y K, Liu Z Q and Wang G H 2001 *Japan. J. Appl. Phys.* **40** 1339
[25] Nagase T, Umakoshi Y and Sumida N 2002 *Mater. Sci. Eng.* A **323** 218
[26] Rodriguez C, Barbiric D A, Pepe M E, Kovacs J A, Alonso J A and Hojvat de Tendler R 2002 *Intermetallics* **10** 205
[27] Fleischer R L, Price P B and Walker R M 1965 *J. Appl. Phys.* **36** 3645
[28] Bitensky I S and Parilis E S 1987 *Nucl. Instrum. Methods* **21** 26
[29] Johnson R E, Sundqvist B U R, Hedin A and Fenyö D 1989 *Phys. Rev.* B **40** 49
[30] Lesueur D and Dunlop A 1993 *Radiat. Eff. Defects Solids* **126** 163
[31] Seitz F and Koehler J S 1956 *Solid State Phys.* **2** 305
[32] Chadderton L T and Montagu-Pollok H M 1969 *Proc. R. Soc.* A **274** 239
[33] Martynenko Yu V and Yavlinskii Yu N 1983 *Sov. Phys.—Dokl.* **28** 391
[34] Toulemonde M, Dufour C and Paumier E 1992 *Phys. Rev.* B **46** 14362
[35] Toulemonde M, Paumier E and Dufour C 1993 *Radiat. Eff. Defects Solids* **126** 407
[36] Szenes G 1995 *Phys. Rev.* B **51** 8026
[37] Dufour C, Wang Z G, Levalois M, Marie P, Paumier E, Pawlak F and Toulemonde M 1996 *Nucl. Instrum. Methods* B **107** 218
[38] Volkov A and Borodin V A 1996 *Nucl. Instrum. Methods* B **107** 172
[39] Volkov A and Borodin V A 1998 *Nucl. Instrum. Methods* B **146** 137
[40] Bringa E M and Johnson R E 2002 *Phys. Rev. Lett.* **88** 165501
[41] Faupel F, Frank W, Macht M-P, Mehrer H, Naundorf V, Rätzke K, Schober H R, Sharma S K and Teichler H 2003 *Rev. Mod. Phys.* **75** 237
[42] Ryazanov A I, Trinkaus H and Volkov A E 2000 *Phys. Rev. Lett.* **84** 919
[43] Frank W 1997 *Defect Diffus. Forum* **143** 695
[44] Dunlop A, Jaskierowicz G and Kopcewicz M 2003 at press
[45] Kopcewicz M, Jackiewicz E, Zaluski L and Zaluska A 1992 *J. Appl. Phys.* **71** 3997
[46] Trinkaus H and Ryazanov A I 1995 *Phys. Rev. Lett.* **74** 5072
[47] Trinkaus H 1996 *Nucl. Instrum. Methods* B **107** 155
[48] Ruuskanen P, Deribas A, Shtertser A and Korkala T 1998 *J. Magn. Magn. Mater.* **182** 185
[49] Spaepen F 1977 *Acta Metall.* **25** 407
[50] Ostwald W 1897 *Z. Phys. Chem.* **22** 289
[51] Stanski I N and Totomanow D 1933 *Z. Phys. Chem.* **163** 399
[52] Duvall G E and Graham R A 1977 *Rev. Mod. Phys.* **49** 523
[53] Keller A, Hikosaka M, Rastogi S, Toda A, Barham P J and Goldbeck-Wood G 1994 *J. Mater. Sci.* **29** 2579
[54] Knorr K, Macht M P, Freitag K and Mehrer H 1999 *J. Non-Cryst. Solids* **250–252** 669